

46. ATTENUATION MEASUREMENTS FROM VERTICAL SEISMIC PROFILE DATA: LEG 104, SITE 642¹

James T. Rutledge² and Hugh Winkler³

ABSTRACT

In-situ seismic attenuation was measured through the upper basalt series using vertical seismic profile (VSP) data collected on ODP Leg 104 at the Vøring Plateau, located along the Norwegian continental margin. Assuming a constant Q model, measurements were made using the spectral ratio method over the bandwidth 7.8 to 62.5 Hz. An effective attenuation of 2.7×10^{-4} dB·s/m $\pm 0.6 \times 10^{-4}$ (Q -effective = 25) was measured over a 525-m interval. Apparent attenuation due to intrabed multiple reflections was computed using synthetic VSP data generated from a well log-derived impedance model. The contribution of apparent attenuation can account for all of the observed attenuation in the upper basalt series. Further, the computed apparent attenuation was found to vary with frequency f as $f^{0.9}$ over the bandwidth 7.8 to 62.5 Hz, indicating that the initial assumption of constant Q was not valid. Q -apparent was computed at two frequencies: at 30 Hz Q -apparent = 55, and at 60 Hz Q -apparent = 29. Within our range of error, intrinsic attenuation in the upper basalt series is less than 0.6×10^{-4} dB·s/m (Q -intrinsic > 115).

INTRODUCTION

Vertical seismic profile (VSP) data provide an easy means of measuring *in-situ* changes in the amplitude and frequency content of a wave traveling through a known stratigraphy. Several recent studies have used VSP data for extracting *in-situ* seismic attenuation through a variety of sedimentary rock types (Ganley and Kanasewich, 1980; Hauge, 1981; Kan et al., 1982; Newman and Worthington, 1982; Stainsby and Worthington, 1985). We have made *in-situ* attenuation measurements through a sequence of basalt flows using the VSP data collected on Leg 104 of the Ocean Drilling Program's (ODP's) investigation of the Vøring Plateau located along the Norwegian continental margin. The VSP experiment was conducted in Hole 642E. We believe these to be the first published results of *in-situ* seismic attenuation through a basalt stratigraphy at sea or on land.

The interval over which VSP data were collected lies nearly entirely within the upper basalt series (Fig. 1). This section manifests itself on seismic reflection profiles as a sequence of seaward-dipping reflectors bounded below by the prominent reflector K (Talwani et al., 1983; Hinz et al., 1984). The stratigraphy of the upper basalt series encountered at Site 642 consists of 120 flows. Interbedded volcanoclastic sediments make up about 4% of the section. The flows are of tholeiitic composition and vary in texture from massive fine grained to vesicular medium grained. Laboratory measurements of velocity and density made on core from the hole suggest that variation of acoustic impedance between both the two flow types and the volcanoclastic sediments is the cause of the strong reflectors observed in the upper basalt series (Eldholm, Thiede, Taylor, et al., 1987).

THE VSP METHOD

Vertical seismic profiling at sea involves the recording of seismic signals transmitted from near the sea surface to a vertical array of seismometers placed in a borehole. The data are acquired by placing a movable, usually three-component seismometer (geophone) downhole and recording signals transmitted from

a seismic energy source. The geophone tool is coupled against the borehole wall by extension of a locking arm for each transmission of the energy source and then incrementally moved up-hole until signals have been recorded at numerous locations from the bottom to the top of the well.

THE SITE 642 VSP DATA SET

The ODP Site 642 VSP experiment is discussed in detail in Eldholm, Thiede, Taylor, et al. (1987). What follows is a brief description of the VSP survey and data set pertinent to our measurements.

The VSP experiment covered a 660-m interval from 451 to 1111 m below sea floor (mbsf) with a geophone spacing of 15 m. Water depth at the site was 1289 m. The seismic source was a high-pressure air gun (Bolt Model 1500C) suspended at 9.15 m water depth from a buoy located about 24.5 m from the drill ship. A hydrophone was positioned at 150 m water depth for monitoring the consistency of the source input signal. Unfortunately, due to recording instrument problems, a useful monitor signal from the hydrophone was not recorded. Although source repeatability is critical in making attenuation measurements, it is not generally a problem with marine air guns (Balch and Lee, 1984). Each firing of the air gun was initiated at the same location and at a pressure of 1800 psi (12.4 MPa). We therefore consider it reasonable to assume that the source input signal was constant throughout the VSP experiment.

The seismic traces were digitally recorded at a 1-millisecond (ms) sample interval for a duration of 6 seconds (s). Because signal content above 60 Hz is negligible, the data were bandpass-filtered between 10 and 60 Hz and resampled at 4 ms. The vertical component of the filtered data was used in processing for attenuation (Fig. 1).

ATTENUATION ANALYSIS

Extraction of seismic attenuation values from VSP data is done by measuring changes in amplitude of compressional P -wave first arrivals corresponding to direct travel path from source to receiver positions. Our attenuation analysis follows that of Hauge (1981).

Many observed data indicate that the logarithm of seismic pulse amplitude decays as a linear function of frequency in homogeneous material. Mathematically we can express the spatial

¹ Eldholm, O., Thiede, J., Taylor, E., et al., 1989. *Proc. ODP, Sci. Results*, 104: College Station, TX (Ocean Drilling Program).

² Los Alamos National Laboratory, Los Alamos, NM.

³ Institute for Geophysics, University of Texas, Austin, TX.

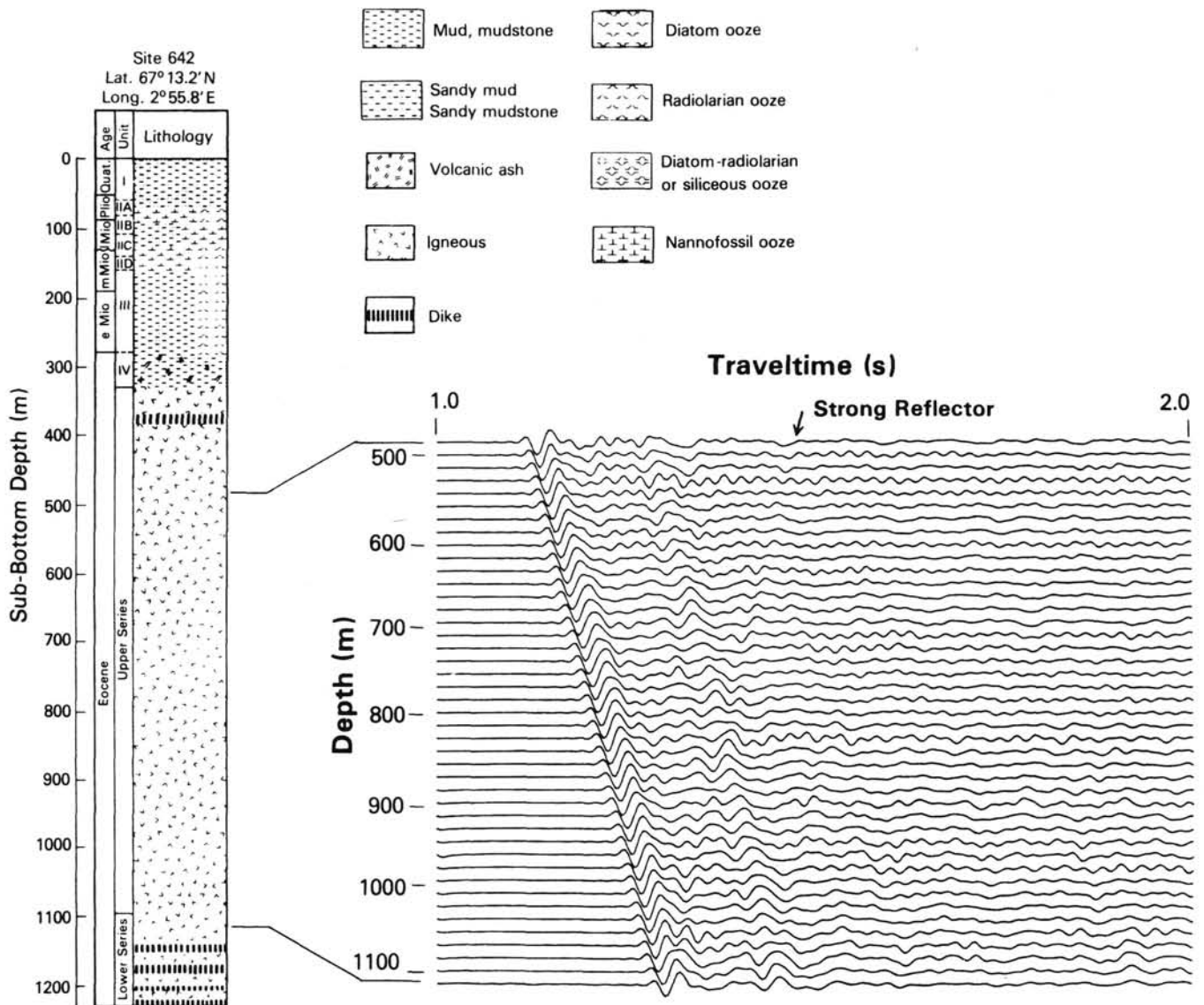


Figure 1. Vertical component VSP data, bandpass-filtered 10 to 60 Hz, shown with generalized stratigraphic section of ODP Leg 104, Site 642. One second of data is displayed from 481 to 1111 mbsf. (Stratigraphic section adapted from Eldholm, Thiede, Taylor et al., 1987).

decay of a plane wave of frequency f propagating along the z -axis as

$$A_z = A_o \exp [-\pi Z f / Q(f) V(f)], \quad (1)$$

where A_o and A_z are the peak amplitude values at some reference location and at some given distance Z from the reference location, respectively (Aki and Richards, 1980). $V(f)$ is the P -wave velocity and $Q(f)$ the dimensionless specific quality factor. We assume in our analysis that Q is constant over the frequency band of our measurements. Constant Q implies that the loss of pulse energy per cycle is equal for all frequencies. Numerous citations of experimental work supporting this relationship are given in review papers by Atwell and Ramana (1966) and Hamilton (1972, 1976). Results from previous near-surface *in-situ* attenuation studies by McDonal et al., (1958), Tullis and Reid (1969), and Newman and Worthington (1982) also validate the constant Q model of attenuation. Although, by arguments of causality, velocity must be dispersive with Q constant (Futter-

man, 1962; Kjartansson, 1979), we assume it also to be constant over our limited bandwidth of 10 to 60 Hz.

In measuring attenuation from near-offset VSP data, we assume vertical incidence of the recorded waveform at each geophone position. Using a linear superposition, constant Q model, the spatial decay of amplitude between depths Z_0 and Z_1 in a homogeneous section can be expressed as

$$A_1(f) = M_{01} A_0(f) \exp [-\pi(Z_1 - Z_0)f / QV]. \quad (2)$$

Equation (2) requires that the geophone instrument's frequency response and source input signal be constant throughout the VSP experiment. M_{01} is a frequency-independent factor that can include amplitude decay due to wavefront spreading, amplitude loss due to simple reflection at an interface, and any recording instrument gain changes between depths Z_0 and Z_1 .

We can rewrite Equation (2) as

$$A_1(f) = M_{01} A_0(f) \exp [-B_{01} f], \quad (3)$$

where B_{01} is called the cumulative attenuation between depths Z_0 and Z_1 . Cumulative attenuation can be isolated by taking the natural logarithm of the amplitude spectral ratios:

$$\ln [A_1(f)/A_0(f)] = \ln M_{01} - B_{01}f. \quad (4)$$

The resultant linear function of frequency has a negative slope B_{01} and intercept $\ln M_{01}$. This is the basis of the spectral ratio method of attenuation analysis. In applying this method we compute spectral ratios between the first arrival spectra at each depth position and the first arrival spectrum at some upper reference depth. A least-squares slope is fitted to each spectral ratio and the resultant cumulative attenuation values are plotted versus depth. The cumulative attenuation values are first converted to units of dB/Hz by multiplying each slope value by 8.686 ($= 20 \log_{10} e$). From the cumulative attenuation vs. depth curve we compute a spatial attenuation value K , with units dB/s/m, where equation (2) could also be rewritten as

$$A_1(f) = M_{01} A_0(f) \exp [-K(Z_1 - Z_0)f]. \quad (5)$$

Attenuation values (K) are determined as slopes of linear trends in the cumulative attenuation curve over selected depth intervals. A change in slope should correspond to variations in the attenuation properties with depth. From the equations shown above, it is also possible to derive Q or attenuation values over any interval of interest from a single spectral ratio calculation. In practice, however, the measurements are not made through a section of homogeneous rock and as a result the spectral ratios can strongly deviate from a linear function due to local interference effects. By computing and plotting cumulative attenuation values at every depth, one can examine the scatter of values with depth and determine accuracy and degree of spatial resolution possible in measuring *in-situ* attenuation.

Scattering and Interference

The presence of layering (or any inhomogeneity) complicates the above attenuation analysis because the layered structure's frequency response is included in the attenuation measurements. Layering can result in an apparent attenuation due to scattering and erratic variations of frequency response at each geophone position, due to interference effects.

A wave propagating through a structure with a rapidly varying seismic impedance undergoes many short-path multiple reflections, a form of scattering. The resultant first arrival observed at some depth is the coherent sum of many complex travel paths between the source and receiver and hence is delayed with respect to the true direct travel path (O'Doherty and Anstey, 1971; Stewart et al., 1984). Upon transmission through thin layers, short-wavelength (high-frequency) signal components tend to be extinguished by destructive interference of multiple reflections while long-wavelength signal components coherently sum. This loss of higher frequencies from the first arrival is an apparent attenuation which can closely resemble intrinsic attenuation (O'Doherty and Anstey, 1971; Schoenberger and Levin, 1974, 1978; Spencer et al., 1977, 1982; Richards and Menke, 1983; Menke, 1983; Banik et al., 1985a).

The attenuation (K) that we measure from the field data cumulative attenuation curve must be considered an effective attenuation $K_E(f)$, since there can be an unknown contribution from intrabed multiples. The effective attenuation can be expressed as the sum of the intrinsic and apparent attenuations; i.e.,

$$K_E(f) = K_I(f) + K_A(f). \quad (6)$$

It is the measurement of intrinsic attenuation $K_I(f)$ which we feel justified in assuming to be independent of frequency (a constant Q model) based on previous work of other investigators which we have cited above. The apparent attenuation $K_A(f)$, associated with intrabed multiple reflections, on the other hand, can be expected to vary with frequency. Spencer et al. (1977), Menke (1983) and Banik et al. (1985b) have shown that for various stochastic models of random impedance $K_A(f)$ will vary as $f^{1.0}$. For more correlated impedance structures (i.e., with an increasing degree of periodic structures) the power of frequency dependence on $K_A(f)$ will tend to decrease from 1.0 (Menke, 1983). Apparent attenuation can be calculated separately by applying the same attenuation measurement techniques to synthetic VSP seismograms that are computed using the known impedance structure with $K_I(f)$ set to zero (Ganley and Kanasevich, 1980). We can thereby determine the relative contributions of $K_A(f)$ and $K_I(f)$ measured from the field data. If the $K_A(f)$ component is significant, its frequency dependence should be determined to extract meaningful values of $K_E(f)$ and $K_I(f)$. It follows that the assumption of Q being independent of frequency may not be valid for *in-situ* seismic attenuation measurements when the relative contribution of $K_A(f)$ is large (Jacobson (1987) presents such a case).

Interference effects are caused by superposition of locally generated reflections with the measured first arrival. The spectra used in calculating spectral ratios are computed from a windowed portion of the seismogram first arrivals. Reflections generated below the receiver position within a distance corresponding to a traveltime of one-half the window duration will be partly included in the true direct arrival. At each geophone position, the frequency characteristic of the reflected waves contaminating the direct arrivals varies as different layering is sampled. Hence, an error associated with local impedance structure is introduced in each spectral ratio. In a homogeneous section, the cumulative attenuation (slope of spectral ratios) vs. depth curve would smoothly increase with a slope equal to the effective attenuation ($K_E(f)$). Reflector interference will cause the cumulative attenuation vs. depth curve to deviate from a linear trend. Interference effects can severely limit the resolution and accuracy of *in-situ* attenuation measurements (Spencer et al., 1982).

MEASUREMENTS OF ATTENUATION

Attenuation measurements were made using the first pulse arrivals of each trace. Approximately 75 ms of data, about $1\frac{1}{2}$ cycles, were separated using a cosine-tapered window. Including the tapered portions to zero, the windowed first arrivals correspond to 32 sample series each of which was fast Fourier transformed to compute the amplitude spectra. Spectral ratios were computed over the frequency band 7.8 to 62.5 Hz. The signal-to-noise ratio over this band ranged from 20 dB to plus 40 dB. The depth of the reference seismogram used in calculating spectral ratios was 496 mbsf. The spectra of the seismograms recorded at the three receiver positions above 496 mbsf varied erratically and were therefore not useful. A sample windowed pulse and its corresponding spectrum and spectral ratio are shown in Figure 2.

Cumulative attenuation vs. depth is shown in Figure 3. Strong interference effects cause the large scatter in data with depth. An effective attenuation K_E of 2.7×10^{-4} dB·s/m $\pm 0.6 \times 10^{-4}$ was computed as the least-squares slope fit of those data points shown connected in Figure 3. The error given is the standard error in slope determination. We have edited out the six data points below 1021 mbsf because of severe interference effects caused by the strong reflector occurring at the base of the

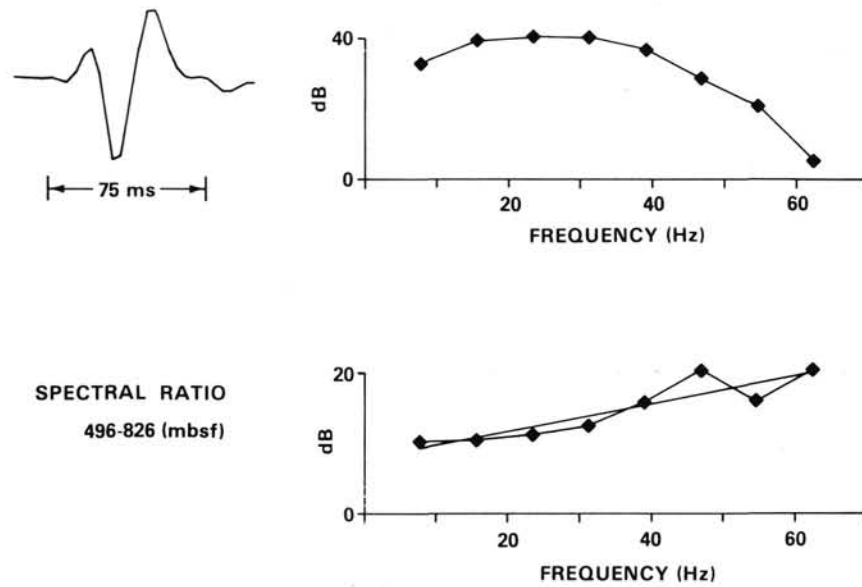


Figure 2. Sample windowed first arrival and corresponding amplitude spectrum at 826 mbsf (above) and spectral ratio (below) computed from the reference first-arrival spectrum at 496 mbsf and the spectrum shown at 826 mbsf. The reciprocal of the spectral ratio shown in equation 4 is plotted to give a positive slope. The least-squares slope fit of the spectral ratio is shown, which yields the effective cumulative attenuation occurring between 496 and 826 mbsf.

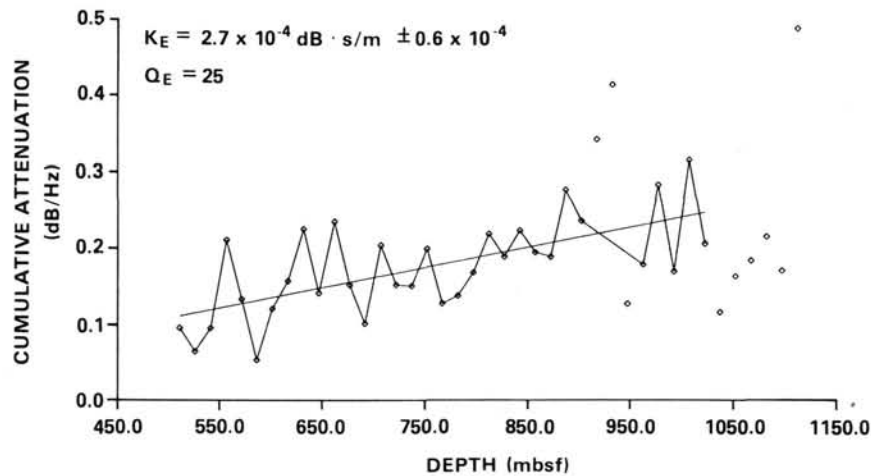


Figure 3. Effective cumulative attenuation of VSP first arrivals within the upper basalt series. The slope, computed by a linear regression over those points shown connected, gives the effective attenuation K_E .

upper basalt series (Fig. 1). The three cumulative attenuation values eliminated at 916 to 946 mbsf depth are thought to vary erratically because of a low signal-to-noise ratio at the high-frequency end of the corresponding spectra. A Q -effective equal to 25 was computed from the spatial attenuation K_E using an average velocity of 4000 m/s. The average velocity was computed over the whole interval of VSP data using traveltimes determined by cross-correlation of the first pulse arrivals. Measurement results are summarized in Table 1.

It should be noted that the slope fit shown in Figure 3 gives a predicted cumulative attenuation value at the reference depth of 496 mbsf, which is significantly greater than zero. For a homogeneous medium the cumulative attenuation trend would go to zero at the reference depth. Due to the presence of reflectors,

the reference first-arrival spectrum, like each downhole first-arrival spectrum, is also contaminated by interference effects. The shape and trend of the cumulative attenuation curve is independent of the reference spectrum, but the curve is shifted upward or downward depending on what interfering reflected signal has contaminated the reference spectrum relative to each downhole spectrum.

We next computed the contribution of scattering to the attenuation measured above using synthetic seismograms. The theoretical response is computed in the frequency domain using a one-dimensional wave equation method similar to that given by Nielsen (1978) and Ganley (1981). A recursive algorithm computes the seismic frequency response at all geophone positions and then Fourier transforms to the time domain to produce the syn-

Table 1. Summary of *in-situ* attenuation measurements in upper basalt series, ODP Hole 642E, assuming constant Q over the bandwidth 7.8 to 62.5 Hz.

	K (dB s/m)	Standard error of K	Q
Effective attenuation	2.7×10^{-4}	$\pm 0.6 \times 10^{-4}$	25
Apparent attenuation (slope between end points)	2.6×10^{-4}	—	25
(linear regression)	2.5×10^{-4}	$\pm 0.5 \times 10^{-4}$	
Intrinsic attenuation	$< 0.6 \times 10^{-4}$	—	> 115

thetic VSP. All multiple reflections are included in the computation.

The synthetic VSP was generated using the impedance structure determined from the sonic and density well logs of Hole 642E. The logs were sampled at 0.305-m (1-ft) intervals and the impedance calculated as the product of sonic velocity and density. Good sonic and density log data were available to 1085 mbsf which is 26 m short of the deepest geophone position occupied during the field experiment. The impedance model extends from the field data reference depth, 496 mbsf, to 1085 mbsf (Fig. 4A). Reflection coefficients were computed at 0.305-m (1-ft) intervals (Fig. 4B) and the resultant synthetic seismogram responses computed at the 15-m geophone spacing of the field data. Since interference effects are strong in the upper basalt series, we computed some additional synthetic seismograms located in halfspaces above and below the series of reflectors represented in Figure 4B. If placed sufficiently far away from any reflectors, the first arrivals of these additional seismograms will not have reflected waveforms superimposed upon them, and therefore allow us to measure a net apparent attenuation through the upper basalt series without the inherent error caused by interference effects.

Cumulative apparent attenuation was computed from the synthetic data using the same measurement parameters applied in the field data analysis except that the reference spectrum corresponds to one of the extra, uncontaminated seismograms at 406 mbsf (Fig. 5). On each end of the synthetic cumulative attenuation curve are three points which do not vary with depth. These values correspond to spectral ratio slopes of the first arrivals unaffected by reflector interference. The slope fit between these end points gives an apparent attenuation K_A of 2.6×10^{-4} dB·s/m. We also computed a linear regression over the same depth points used in the effective attenuation measurements for comparison of the quality of slope fit between synthetic and field data. The linear regression gives a K_A value of $2.5 \times 10^{-4} \pm 0.5 \times 10^{-4}$ dB·s/m. The slope value computed from the end points should be more accurate since it is not affected by the error due to interference. Apparent attenuation measured either way does not significantly differ from the effective attenuation measured from the field data (Table 1). This implies that scattering due to intrabed multiple reflections can account for all the observed attenuation in the upper basalt series.

Computation of intrinsic attenuation using equation 6 gives a value less than the standard errors of effective and apparent attenuation. We give the standard error of effective attenuation as the upper limit of intrinsic attenuation in the upper basalt series (Table 1) since this amount could be accommodated within the measurement error. This corresponds to a Q -intrinsic greater than 115. Laboratory measurements of attenuation on various basalts over the frequency band 3 to 4 kHz give intrinsic attenuation values well below our upper limit (Bradley and Fort, 1966).

As noted above, the apparent attenuation K_A , due to intrabed multiples, can be expected to vary as a function of frequency. Since K_A is by far the dominant component of K_E , we

remeasured the contribution of K_A over two separate frequency intervals to determine its frequency dependence and thereby test if our initial assumption of a constant Q was valid. To reduce errors in our measurements, we computed a series of seismograms in the absence of interference effects. The seismic traces were computed individually in a homogeneous halfspace below a series of reflectors derived from a portion of the impedance model (again, starting at the reference depth 496 mbsf) and the impedance model extended for each subsequent trace. This results in a synthetic VSP data set undergoing a cumulative apparent attenuation without local interference from reflectors below the geophone. In our analysis, we used first-arrival spectra of nine synthetic seismograms computed at 25-m intervals over the lower 200 m of the log-derived model.

To determine the frequency dependence of $K_A(f)$ we can rewrite equation 5 as

$$A_1(f) = M_{01} A_0(f) \exp[-K(Z_1 - Z_0)f^N] \quad (7)$$

where frequency f is now raised to some power N . For a constant Q model, $N = 1$. A plot of $\log[K(Z_1 - Z_0)f^N]$ vs. \log frequency gives a slope equal to N . We have separated the whole exponential term of equation 7 by taking natural logs of average amplitude ratios over two separate octaves of frequency (15.6 to 31.2 and 31.2 to 62.5 Hz). The reference signal corresponds to an impulse of unit amplitude input above the series of reflectors. The attenuation function $[K(Z_1 - Z_0)f^N]$ was plotted against the average frequencies of the two octave intervals (23.4 and 46.9 Hz, respectively) for all nine spectra on a log-log scale (Fig. 6). When computing attenuation from a ratio of single-amplitude values at a given frequency, it is necessary to account for frequency-independent transmission losses occurring across interfaces. The frequency-independent attenuation is termed the compensated transmission loss (Schoenberger and Levin, 1978) and is due to the difference in frequency-independent amplitude loss by reflection at individual interfaces and the frequency-dependent restoration of amplitude by intrabed multiples. We accounted for this loss by normalizing each spectrum with respect to its DC component before computing the amplitude ratios. The power of frequency N was computed by letting the intercepts vary and finding the least-squares slope that best fit all nine curves of Figure 6. We determined an N value of 1.9 ± 0.03 . This implies that K_A or $1/Q$ -apparent varies as $f^{0.9}$, which is close to the linear dependence of $1/Q$ -apparent with frequency predicted by other investigators for random impedance structures. A mean Q -apparent was computed at two frequencies, from the attenuation functions of the nine first-arrival spectra: at 30 Hz Q -apparent = 55 ± 2 , and at 60 Hz Q -apparent = 29 ± 1 . The errors given are the standard error of the mean.

DISCUSSION

Attenuation in the upper basalt series is unusual in that scattering due to intrabed multiples accounts for all the observed loss and further that the Q -apparent is very low ($= 29$ at 60 Hz). Schoenberger and Levin (1978) measured apparent attenuation losses due to intrabed multiples for 31 wells located in a variety of basins worldwide (we presume mostly or all representing sedimentary sections). Assuming a constant Q , they found Q -apparent to range from 125 to 3000 with a mean value of about 325. They also measured the contribution of intrabed multiples to the total-field measured effective attenuation for eight wells and found it to range from 14% to 80%. All but the upper limit case of 80% were below 50%. It is the presence of large and rapid variations of impedance in the upper basalt series that causes the large component of scattering loss. Menke (1983) derives a formula for a medium with impedance varying randomly in which

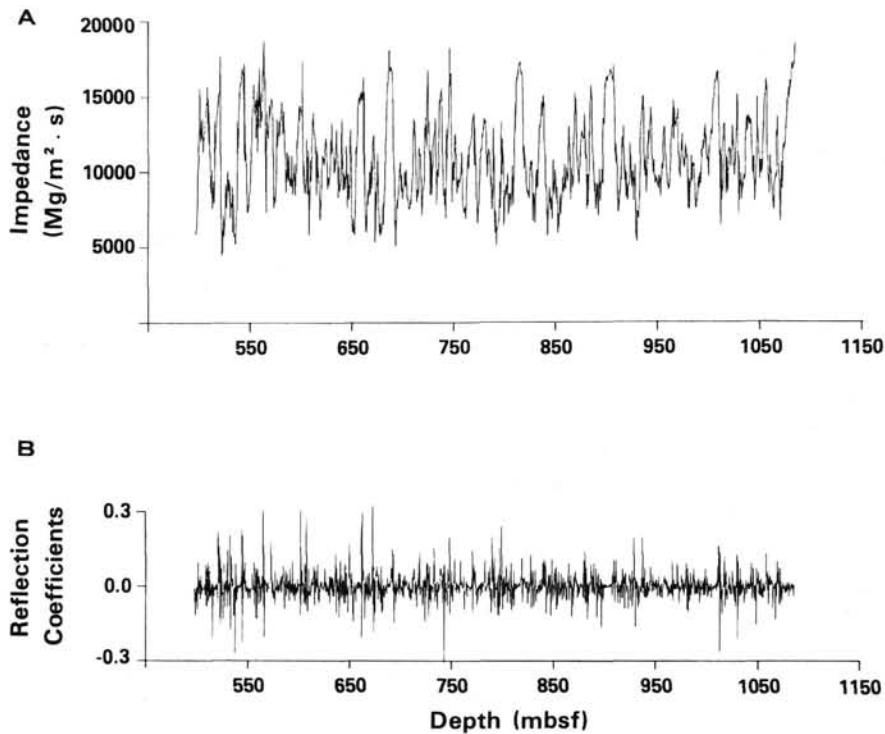


Figure 4. A. Impedance vs. depth over the interval of attenuation measurements as determined from the sonic velocity and bulk density well logs of Hole 642E. B. Reflection coefficient series computed at 0.305 m (1 ft) intervals from the log-derived impedance curve.

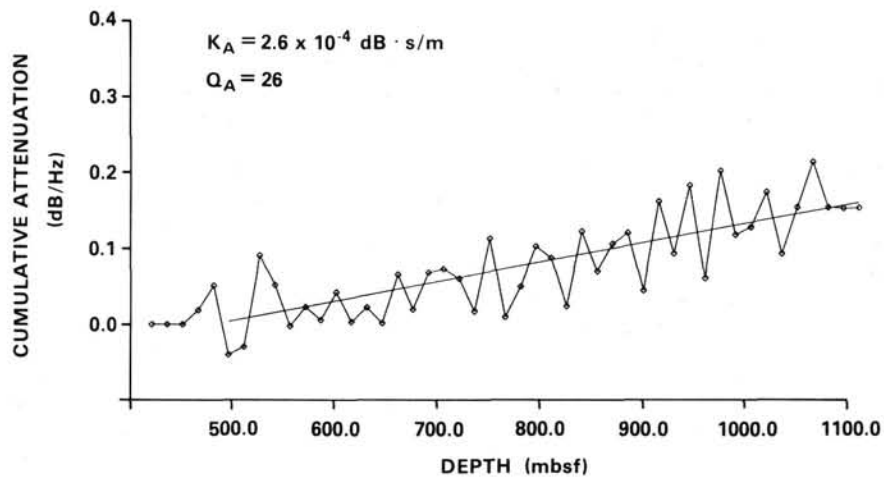


Figure 5. Apparent cumulative attenuation of the synthetic VSP first arrivals. The slope fit and K_A displayed were determined from the end point cumulative attenuation values not contaminated by interference effects. In computing the slope, the zero value on the left-hand side was extrapolated to the shallowest reflector depth of the model (496 mbsf).

$$1/Q\text{-apparent} = (\sigma_i/\bar{i})^2 (\pi f h/\bar{V}) \quad (8)$$

where \bar{i} is the mean impedance of the medium, σ_i the rms fluctuation of impedance, h the layer thickness, \bar{V} the average velocity, and f the frequency. He suggests that a typical value in the

Earth's crust for the fluctuation of impedance with respect to the mean would be about 5% (the quantity squared in equation 8). The log-derived impedance model shown in Figure 4A has a 25% rms fluctuation with respect to the mean. The relationship shown in equation 8 therefore implies that the contribution of

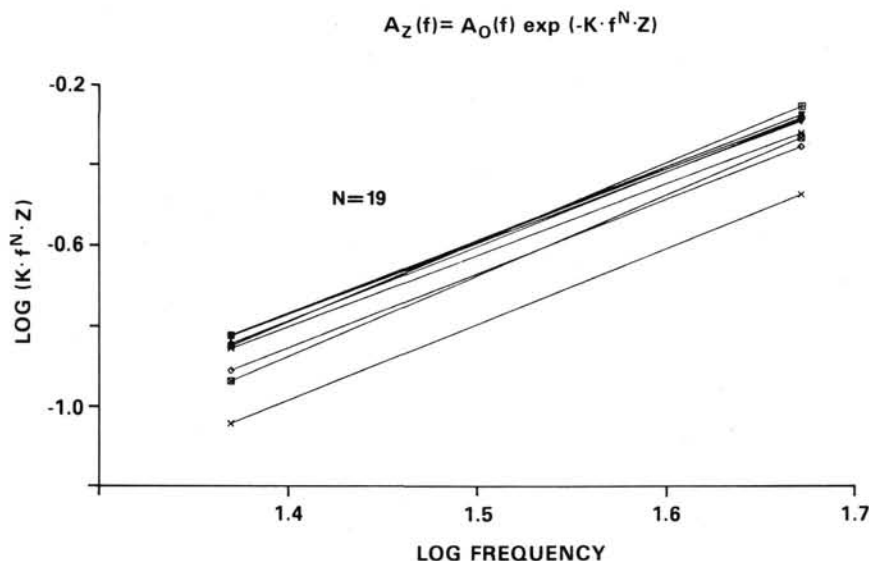


Figure 6. Log-log plot of attenuation function vs. frequency for nine first-arrival spectra at two frequencies.

impedance contrast to apparent attenuation in the upper basalt series is 25 times greater than typical crustal structures.

Finally, Figure 7 shows a comparison of the cumulative attenuation curves for field and synthetic data over the common interval 511 to 1111 mbsf. Oscillations in the field data cumulative attenuation curve should, ideally, be predominantly dependent on the section's impedance structure (Spencer et al., 1982; Dietrich and Bouchon, 1985). A running average (using an 18-m (60-ft) window) of the impedance structure used in generating the synthetic data is also shown in Figure 7. The impedance curve has been shifted uphole about 35 m to match the oscillation of the synthetic cumulative attenuation curve. This correlation between impedance and synthetic data cumulative attenuation demonstrates that the interference effects are due to the reflectors immediately below each geophone position. Differences in magnitude and shape of the cumulative attenuation curves can result from (a) inaccuracies of the log data, (b) model error due to the impedance structure varying away from the borehole, and (c) geophone coupling and source excitation variations during the VSP experiment. The large differences of the cumulative attenuation curves over the six deepest geophone positions (1021 to 1111 mbsf) are a result of the synthetic model only extending to 1085 mbsf. Interference resulting from reflections generated below 1085 mbsf on the field VSP are therefore not represented on the synthetic VSP. Above 1021 mbsf, the cumulative attenuation curves do show a rough correlation, and the residual variances of each curve with respect to its linear fit are nearly equivalent (standard errors given in Table 1 are computed from the residual variances). This implies that the effective attenuation measurement error is predominantly due to interference effects. We therefore consider our measurement and modeling results to be reliable within the inherent error associated with the stratigraphy encountered.

SUMMARY

In-situ seismic attenuation was measured through the upper basalt series from VSP data collected in Hole 642E. Starting with the assumption of a constant Q , the effective attenuation K_E measured over the bandwidth 7.8 to 62.5 Hz equals 2.7×10^{-4} dB·s/m (Q -effective = 25). The contribution of apparent attenuation K_A , or scattering, due to intrabed multiple reflections was computed from synthetic VSP data. Scattering can ac-

count for all of the observed attenuation due to the highly cyclic, large-contrast impedance structure of the upper basalt series. K_A was shown to vary with frequency as $f^{0.9}$ over the bandwidth 7.8 to 62.5 Hz. Since K_A is by far the dominant component of K_E , our initial assumption of constant Q is not valid. Q -apparent at 30 Hz equals 55 and at 60 Hz equals 29. An intrinsic attenuation value less than 0.6×10^{-4} dB·s/m (Q -intrinsic > 115) can be accommodated within the error of effective attenuation.

REFERENCES

- Aki, K., and Richards, P. G., 1980. *Quantitative Seismology, Theory and Methods* (Vol. 1): San Francisco (W. H. Freeman and Co.), 167-185.
- Attewell, P. B., and Ramana, Y. V., 1966. Wave attenuation and internal friction as functions of frequency in rocks. *Geophysics*, 31:1049-1056.
- Banik, N. C., Lerche, I., and Shuey, R. T., 1985a. Stratigraphic filtering, Part 1: Derivation of the O'Doherty-Anstey formula. *Geophysics*, 50:2768-2774.
- Banik, N. C., Lerche, I., Resnick, J. R., and Shuey, R. T., 1985b. Stratigraphic filtering, Part 2: Model spectra. *Geophysics*, 50:2775-2783.
- Balch, A. H., and Lee, M. W., 1984. *Vertical Seismic Profiling: Technique, Applications, and Case Histories*: Boston (International Human Resources Development Corp.), 142-149.
- Bradley, J. J., and Fort, Jr., A. N., 1966. Internal friction in rocks. In Clark, Jr., S. P., (Ed.), *Handbook of Physical Constants* (1966 revised edition): New York (The Geological Society of America, Inc.), 178-193.
- Dietrich, M., and Bouchon, M., 1985. Measurements of attenuation from vertical seismic profiles by iterative modeling. *Geophysics*, 50:931-949.
- Eldholm, O., Thiede, J., Taylor, E., et al., 1987. *Proc. ODP, Init. Repts.*, 104: College Station, TX (Ocean Drilling Program).
- Futterman, W. I., 1962. Dispersive body waves. *J. Geophys. Res.*, 67:5279-5291.
- Ganley, D. C., 1981. A method for calculating synthetic seismograms which include the effects of absorption and dispersion. *Geophysics*, 46:1100-1107.
- Ganley, D. C., and Kanawich, E. R., 1980. Measurement of absorption and dispersion from check shot surveys. *J. Geophys. Res.*, 85:5219-5226.
- Hamilton, E. L., 1972. Compressional wave attenuation in marine sediments. *Geophysics*, 37:620-646.
- _____, 1976. Sound attenuation as a function of depth in the sea floor. *J. Acoust. Soc. Am.*, 56:528-538.

- Hauge, P. S., 1981. Measurements of attenuation from vertical seismic profiles. *Geophysics*, 46:1548-1558.
- Hinz, K., Dostman, H. J., and Hanisch, J., 1984. Structural elements of the Norwegian Sea, continental margin. *Geol. Jahrb.*, A75:193-211.
- Jacobson, R. S., 1987. An investigation into the fundamental relationships between attenuation, phase dispersion, and frequency using seismic refraction profiles over sedimentary structures. *Geophysics*, 52:72-87.
- Kan, T. K., Corrigan, D., and Huddleston, P. D., 1982. Attenuation measurements from vertical seismic profiles. *Geophysics*, 47:466. (Abstract).
- Kjartansson, F., 1979. Constant Q-Wave propagation and attenuation. *J. Geophys. Res.*, 84:4737-4748.
- McDonal, F. J., Angona, F. A., Mills, R. L., Sengbush, R. L., Van Nostrand, R. G., and White, J. E., 1958. Attenuation of shear and compressional waves in Pierre shale. *Geophysics*, 23:421-439.
- Menke, W., 1983. A formula for the apparent attenuation of acoustic waves in randomly layered media. *Geophys. J. Roy. Astron. Soc.*, 75:541-544.
- Newman, P. J., and Worthington, M. H., 1982. *In-situ* investigation of seismic body wave attenuation in heterogeneous media. *Geophys. Prospect.*, 30:337-400.
- Nielsen, P. H., 1978. Calculation of synthetic reflection seismograms in the frequency domain. *Geophys. Prosp.*, 26:399-406.
- O'Doherty, R. F., and Anstey, N. A., 1971. Reflections on amplitudes. *Geophys. Prosp.*, 19:430-458.
- Richards, P. G., and Menke, W., 1983. The apparent attenuation of a scattering medium. *Bull. Seism. Soc. Am.*, 73:1005-1021.
- Schoenberger, M., and Levin, F. K., 1974. Apparent attenuation due to intrabed multiples. *Geophysics*, 39:278-291.
- _____, 1978. Apparent attenuation due to intrabed multiples, II. *Geophysics*, 43:730-737.
- Spencer, T. W., Edwards, C. M., and Sonnand, J. R., 1977. Seismic wave attenuation in nonresolvable cyclic stratification. *Geophysics*, 42:939-949.
- Spencer, T. W., Sonnand, J. R., and Butler, T. M., 1982. Seismic Q-stratigraphy or dissipation. *Geophysics*, 47:16-24.
- Stainsby, S. D., and Worthington, M. H., 1985. Q estimation from vertical seismic profile data and anomalous variations in the central North Sea. *Geophysics*, 50:615-626.
- Stewart, R. R., Huddleston, P. D., Kan, T. K., 1984. Seismic versus sonic velocities: a vertical seismic profiling study. *Geophysics*, 49:1153-1168.
- Talwani, M., Mutter, J., and Hinz, K., 1983. Ocean continent boundary under the Norwegian continental margin. In Bott, M. H. P., Saxov, S., Talwani, M., and Thiede, J. (Eds.), *Structure and Development of the Greenland-Scotland Ridge—new methods and concepts*: New York (Plenum Press), 121-131.
- Tullos, F. N., and Reid, A. C., 1969. Seismic attenuation in Gulf Coast sediments. *Geophysics*, 34:516-528.

Date of initial receipt: 28 March 1987
 Date of acceptance: 15 February 1988
 Ms 104B-193

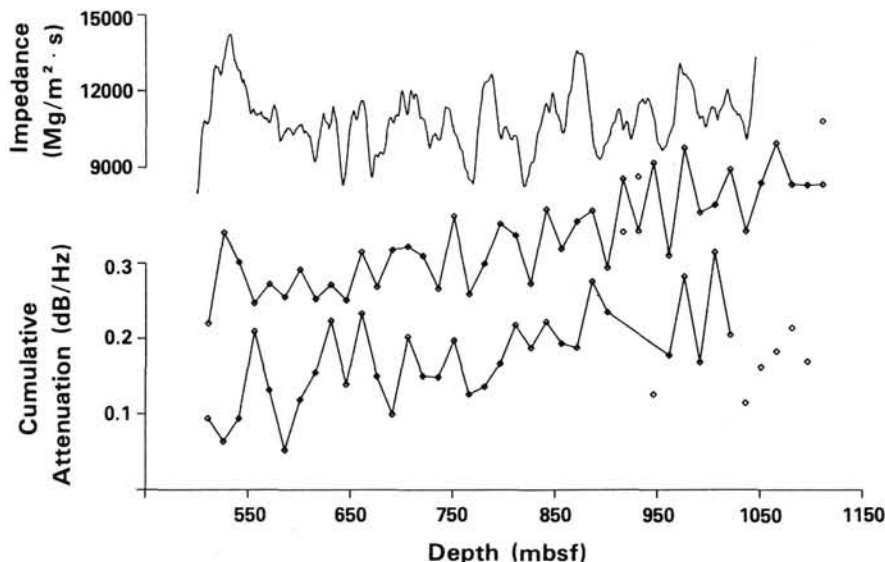


Figure 7. Comparison of the cumulative attenuation curves of the field VSP (bottom), synthetic VSP (center), and the impedance structure (top).